Effects of Thickness and Ag Layer Addition on the Properties of ZnS Thin Films

S.H. Mohamed[a,*], N.M.A. Hadia[a,b], M.A. Awad[a] and Essam R. Shaaban[c]

[a]Physics Department, Faculty of Science, Sohag University, 82524 Sohag, Egypt

[b]Department of physics, College of Science, Jouf University, Jouf, Saudi Arabia

[c]Department of Physics, Faculty of Science, Al-Azahar University, Assiut, 71542, Egypt

(Received April 21, 2018; revised version July 16, 2018; in final form August 13, 2018)

Zinc sulfide (ZnS) thin films, with different thicknesses and different silver (Ag) middle layer thickness, were prepared on glass substrates using thermal evaporation. The structural and optical properties of ZnS thin films were characterized by X-ray diffraction and UV-VIS-NIR spectrophotometer. The X-ray diffraction analyses indicated that ZnS films have cubic structure with (111) preferential orientation, whereas the diffraction patterns sharpen with the increase in the film thickness. The intensities of the Ag peaks increased strongly while the intensities of ZnS peaks decreased when the Ag layer increased to 86 nm. The optical band gap values decreased while the refractive index increased with the increase of the film thickness and Ag layer thickness. These results show that ZnS films are suitable for use as the buffer layer of the Cu(In, Ga)Se_2 solar cells.

DOI: 10.12693/APhysPolA.135.420

PACS/topics: ZnS film, thermal evaporation, buffer layer, effect of thickness, Ag layer thickness

1. Introduction

Zinc sulfide (ZnS) thin films are considered as one of the best materials for various applications such as photovoltaic and solar cells applications [1, 2], warm white lighting emitting devices [3], lasers and sensors [4], optical filters [5] as well as antireflection coatings [6].

Buffer layers are commonly used in the optimization of thin-film solar cells. For $CuInSe_2$- and CdTe-based solar cells, multilayer transparent conductors (TCOs, e.g., ZnO or SnO_2) are generally used in conjunction with a CdS heterojunction layer. Optimum cell performance is usually found when the TCO layer in contact with the CdS is very resistive or almost insulating. In addition to affecting the open-circuit voltage of a cell, it is commonly reported that buffer layers affect stress-induced degradation and transient phenomena in CdTe- and $CuInSe_2$-based solar cells [7]. Nowadays, ZnS is considered one of the best materials for the Cu(In,Ga)Se_2 (CIGS) solar cells among possible alternative buffer layers. In comparison with CdS, the advantages of ZnS include its nontoxic and environmentally safe handling as well as its ability to provide better lattice matching to CIGS absorbers [8]. The thickness of the ZnS buffer layer and the addition of Ag layer in the ZnS heterojunction are affecting the properties of the buffer layer and therefore the whole performance of the solar cell. Therefore, in this paper we report both the effect of thickness and Ag middle layer addition on optical properties of ZnS buffer layer.

*corresponding author; e-mail: abo_95@yahoo.com

2. Experimental details

ZnS thin films with different thicknesses (390, 621, and 801 nm) were prepared by thermal evaporation in a coating unit (Auto306FL400). The films were deposited on glass substrates by putting ZnS powder (99.999% purity, MV Lab. INC., USA) in the melting-boat, then ZnS powder was heated thermally until evaporated, and deposited on the substrates. Rotary and diffusion pumps were used to reach the pressure of $\approx 10^{-5}$ mbar. The deposition rate was ≈ 4 nm/s.

ZnS/Ag/ZnS multilayer thin films were prepared also by thermal evaporation as follows. At first, a layer of ZnS was deposited on the glass substrates with thickness of ≈ 310 nm. After that, Ag was placed in the melting-boat and in the same way Ag was heated and evaporated on the ZnS layer with the same deposition rate and with ≈ 19 nm thickness. Finally, a second ZnS layer of ≈ 310 nm thickness was deposited on the Ag layer to obtain multilayer of ZnS/Ag/ZnS with 310/19/310 thicknesses. In the same way, a second ZnS/Ag/ZnS multilayer system of thicknesses 310/86/310 was prepared. For comparison a third film was prepared without adding Ag layer and its accumulated thickness was ≈ 621 nm (i.e. 310/0/310).

The crystallographic structure was examined using X-ray diffraction (XRD), and Cu K_α radiation ($\lambda = 1.541838$ Å) was used with normal focus. The optical transmittance T and reflectivity R on ZnS/Ag/ZnS films were measured using photospectrometer in the wavelength λ range of 200–2500 nm at normal incidence. The film thickness d and refractive index n were calculated according to the transmission maximum and minima with the method described by Swanepoel. The optical energy gap E_g of the films was deduced by using Tauc's law.

3. Results and discussion

3.1. Effect of thickness on structural and optical properties of ZnS films

The XRD patterns of the ZnS films with different thicknesses are shown in Fig. 1a–c. The XRD pattern of ZnS film with thickness of 390 nm exhibits one main diffraction peak at 28.25° as well as some tiny peaks which can be all indexed to cubic ZnS (JCPDS card no. 80-0020). This indicates that the film is highly textured with preferred orientation around (111). As the thickness increased to 621 nm, and then to 801 nm the intensity of the (111) diffraction peak increased and no new peaks were observed. This indicates that the texturing of the ZnS films, around the (111) peak, enhanced with increase in the film thickness. The grain sizes G of ZnS films were calculated from the (111) peak using Scherrer's formula [9]:

$$G = \frac{k\lambda}{\beta \cos(\theta_c)}, \tag{1}$$

where k denotes the Scherrer constant ($k = 0.94$), λ is the wavelength of the Cu K_α radiation ($\lambda = 1.541838$ Å) and β is the full width at half maximum (FWHM) of a Gauss fit. The accuracy of this method is dependent on the success in measuring the actual width at half intensity of a diffraction peak [10]. It is important to realize that the Scherrer formula provides a lower bound on the particle size. That is because there are many factors that can contribute to the width of a diffraction peak in addition to particle size, the most important of these are usually inhomogeneous strain and instrumental effects. If all of these other contributions to the peak width were zero, then the peak width would be determined solely by the particle size, and the Scherrer equation would apply. If the other contributions to the width are nonzero, then the particle size can be larger than that predicted by the Scherrer formula, with the extra peak width coming from the other factors. In this data the precision of the obtained grain size is not high because the influences of film stress on lattice and on the instrumental peak broadening of the peak width have not been considered [10].

The obtained grain size values are listed in Table I. The grain size increases with film thickness indicating that the increase in thickness provides a better crystallization for the films.

TABLE I

Full width at half maximum (FWHM), grain size G and optical band gap E_g of ZnS films with different thicknesses.

Thickness [nm]	FWHM	G [nm]	E_g [eV]
390	0.52169	16.42	3.58 ± 0.02
621	0.43987	19.46	3.46 ± 0.02
801	0.37601	22.79	3.31 ± 0.02

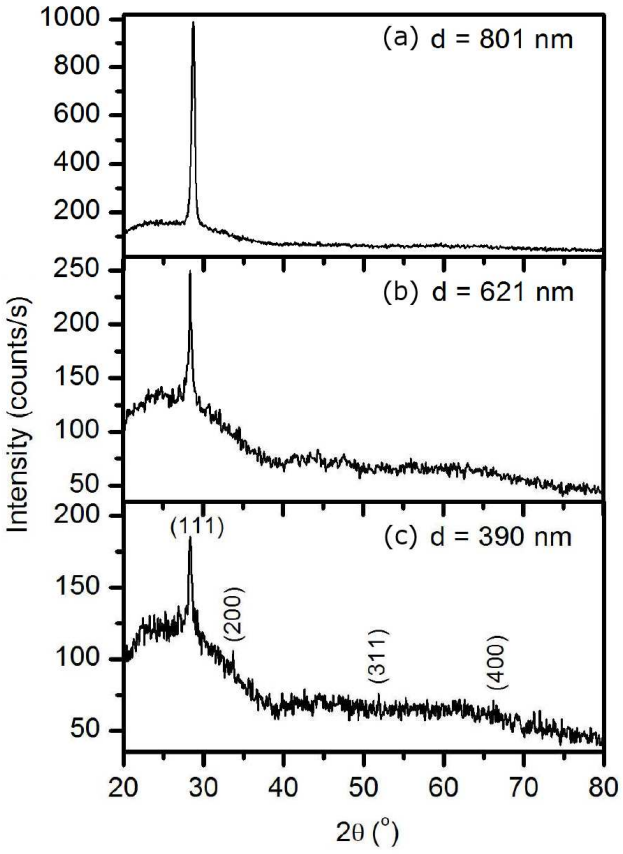

Fig. 1. XRD patterns of the ZnS films with different thicknesses.

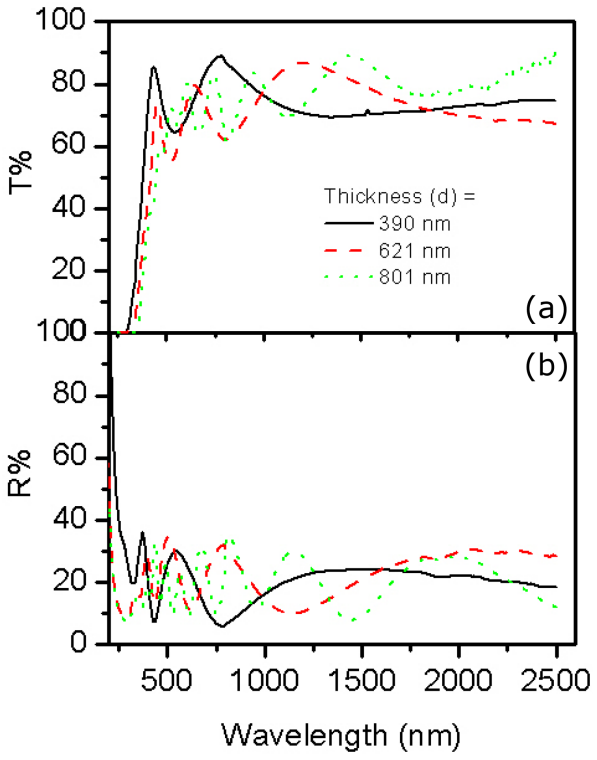

Fig. 2. The transmittance (a) and reflectance (b) spectra of ZnS films with different thicknesses.

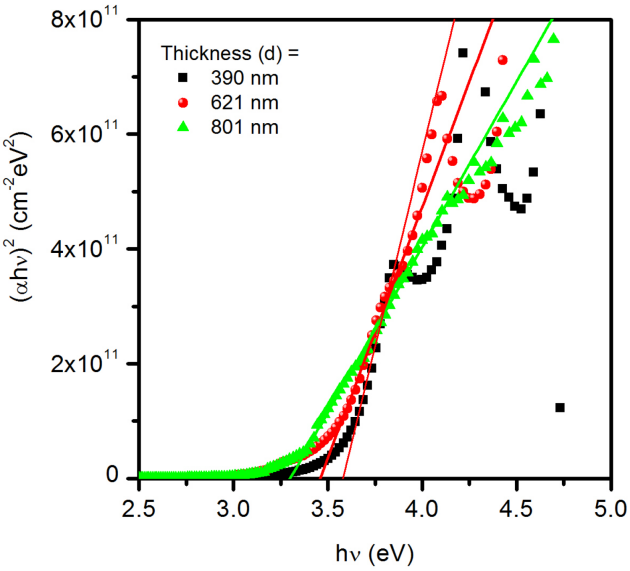

Fig. 3. $(\alpha h\nu)^2$ versus $h\nu$ plots of ZnS with different thicknesses.

The transmittance and reflectance spectra of ZnS films with different thickness are shown in Fig. 2. The spectra reveal that films, grown under the same parametric conditions, have high transmittance in the visible and near infrared regions. However, the transmittance in the ultraviolet region is low. A strong absorption edge is observed in the neighbourhood of $\lambda = 440$ nm. The maximum absorption edge shifts towards the longer wavelength with increasing film thickness. This suggests the decrease in the band gap with the increasing thickness. The overall transmittance decreased slightly with the film thickness. This is because of that in case of thicker films more atoms are present in the film so more states will be available for the photons to be absorbed [11].

The optical band gap values, E_g, are calculated by assuming an indirect transition between the edges of the valence and the conduction bands, using the equation

$$(\alpha h\nu)^2 = A(h\nu - E_g), \tag{2}$$

where α is the absorption coefficient and A is a constant. By plotting $(\alpha h\nu)^2$ versus $h\nu$ and extrapolating the linear region of the resulting curve, E_g can be obtained as shown in Fig. 3. The calculated E_g values are written in Table I. The E_g values decrease from 3.58 ± 0.02 to 3.31 ± 0.02 eV with increase of the film thickness from 390 to 801 nm. This observation has been reported previously be many researchers [12–14]. Prathap et. al. [13] reported a decrease in band gap from 3.85 to 3.54 eV with increase in the thickness of the thermally evaporated ZnS films from 100 to 600 nm. Mohamed et al. [12] reported a decrease in band gap values of the electron beam evaporated ZnS films from 3.70 to 3.43 eV with increase of the thickness from 50 nm to 400 nm. Also, a decrease in band gaps values from 3.62 eV to 3.52 eV were reported by Echendu and Dharmadasa [14] for electrodeposited ZnS films ranged from 400 nm to 700 nm, respectively. It is known that the optical band gap of semiconductors is affected by defects, residual strain, disorder at the grain boundaries, charged impurities, and particle size confinement [12, 13]. The compressive strain results in an increase in the optical band gap due to the compressed lattice of the film whereas the tensile strain results in a decrease of band gap because of the elongated lattice. As an enhancement in film crystallinity with increasing thickness is obtained, the reduction in band gap can be primarily ascribe to the increase in particle size together with the possible stresses which arises during deposition.

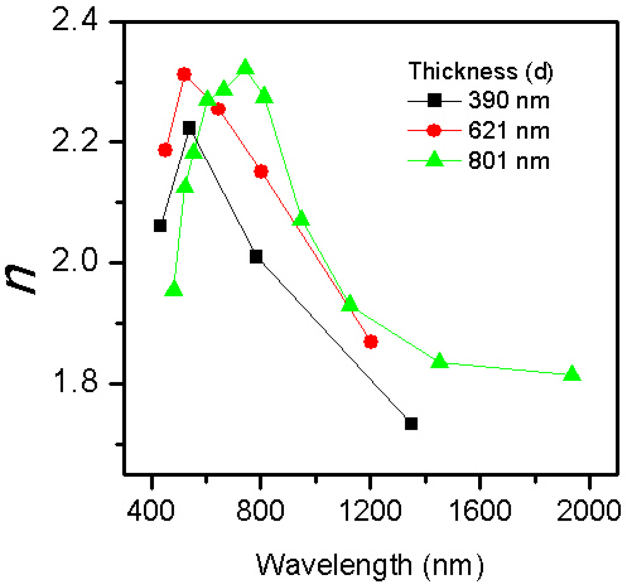

Fig. 4. Variations of the refractive index of ZnS with different thicknesses as functions of wavelength.

The refractive index values, n, of ZnS films prepared with different thicknesses were calculated from the spectral transmittance using the Swanepoel method [15, 16]. The results are shown in Fig. 4 as a function of wavelength. The refractive index increases with increase of film thickness due to the densification associated with more building blocks for thicker films.

3.2. Effect of Ag layer addition on structural and optical properties of ZnS films

The crystallographic structure was examined using XRD. The qualitative XRD spectra for ZnS/Ag/ZnS films prepared with different Ag layer thicknesses are depicted in Fig. 5. Figure 5a shows the XRD pattern of ZnS thin film without Ag layer (310/0/310), there is a main peak around 28.67° which corresponds to the (111) orientation of the cubic ZnS structure (JCPDS Card no. 80-0020). Upon the addition of 19 nm Ag layer, new crystalline peaks are observed as shown in Fig. 5b. The peaks are corresponding to (111), (200), (220), and (311) orientations of the cubic Ag structure (JCPDS Card

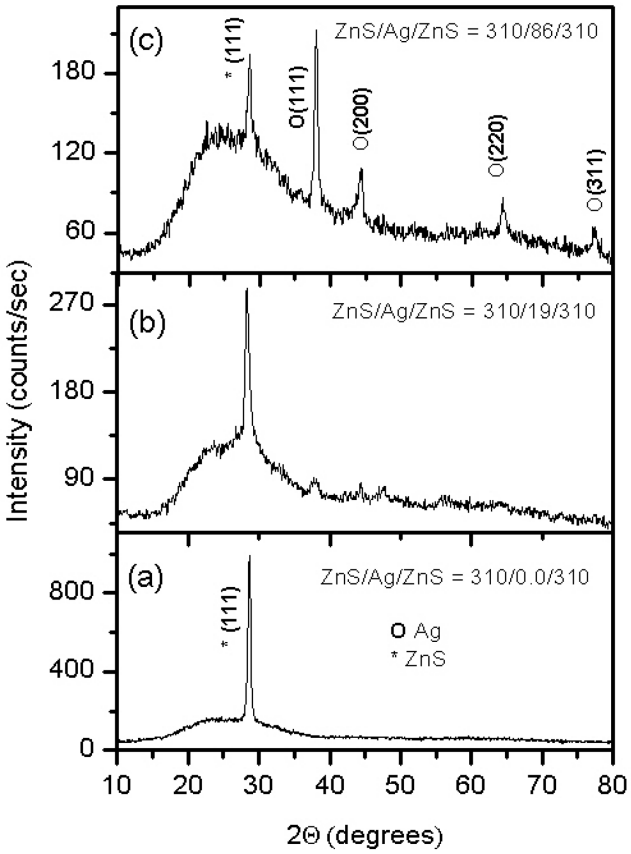

Fig. 5. XRD patterns of the ZnS/Ag/ZnS multilayer films with different Ag thicknesses.

no. 04-0783). The intensities of the Ag peaks increase strongly when the Ag layer increases to 86 nm, whereas the intensity of the ZnS peak decreases.

It is worth mentioning that the Ag layer is obviously polycrystalline. However, the second ZnS layer grown on the top of Ag is still highly textured with preferred orientation around (111). Procedures, which control the texture developmen, are diffusion of surface atoms, probability of precursor sticking, interactions of energetic particles with the surface of the substrate as well as with the surface of growing film and grain growth. The proposed theoretical models for texture depend on (i) effects of ion impact, (ii) anisotropic surface energy and surface diffusion, (iii) residual stresses accompanying with a volume-proportional elastic energy, and (iv) effects of recrystallization inside the bulk of the film [17]. However, the decisive point is the definite anisotropic growth rate which favours the growth texturing direction over those in the basal plane. This can be produced by the energetics of the cubic crystallographic structure of ZnS, which is an intrinsic property for ZnS.

The grain size of ZnS in the ZnS/Ag/ZnS multilayer was calculated by the Scherrer equation [9] and listed in Table II. The grain size decreases with increasing Ag layer thickness. This observation has been reported previously in the ZnO/Ag/ZnO multilayer system [18].

TABLE II

Grain size G and optical band gap E_g of ZnS/Ag/ZnS multilayer system.

ZnS/Ag/ZnS [nm]	G nm	E_g [eV]
310/0/310	19.46	3.61 ± 0.02
310/19/310	18.31	3.45 ± 0.02
310/86/310	16.3	3.24 ± 0.02

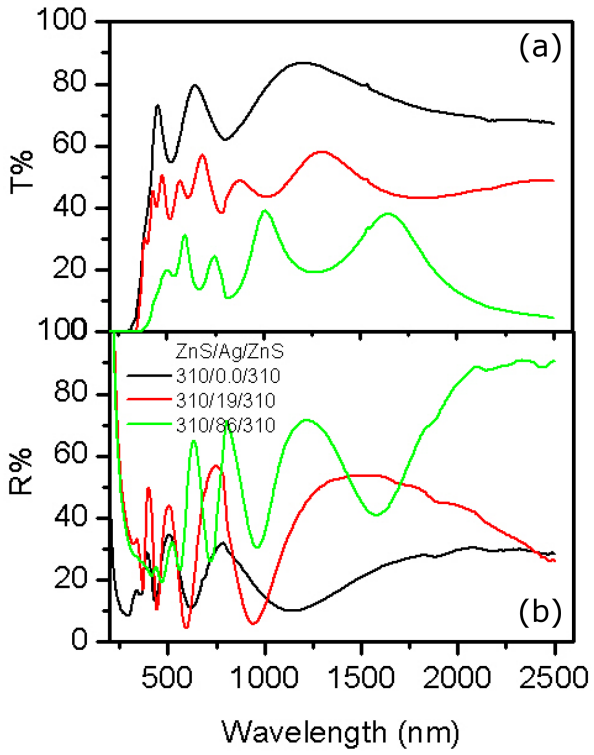

Fig. 6. The transmittance (a) and reflectance (b) spectra of ZnS/Ag/ZnS multilayer films with different Ag thicknesses.

Figure 6a and b shows the variations of transmittance and reflectance as a function of wavelength in the range 200–2500 nm for the ZnS/Ag/ZnS system. It is seen from Fig. 6a that the transmittance of the single ZnS layer is very high over the entire wavelength range. As the thickness of the Ag layer increases, the transmittance of the multilayer system decreases in both the visible and the near infrared regions. The most pronounced decrease is found in the NIR due to the increase in reflection caused by the free electrons in the Ag layer (Fig. 6b). The onset of absorption is shifted to the higher wavelengths as Ag thickness increases.

The E_g values of the ZnS/Ag/ZnS multilayer system were calculated from $(\alpha h\nu)^2$ versus $h\nu$ plot as shown in Fig. 7. The calculated E_g values are listed in Table II. The E_g of ZnS/Ag/ZnS multilayer system decreases with increase of Ag thickness. The same trend was reported also by many research groups [19–22] for various metal-oxide/metal/metal-oxide multilayer films. They elucidated this type of decrease to the many-body

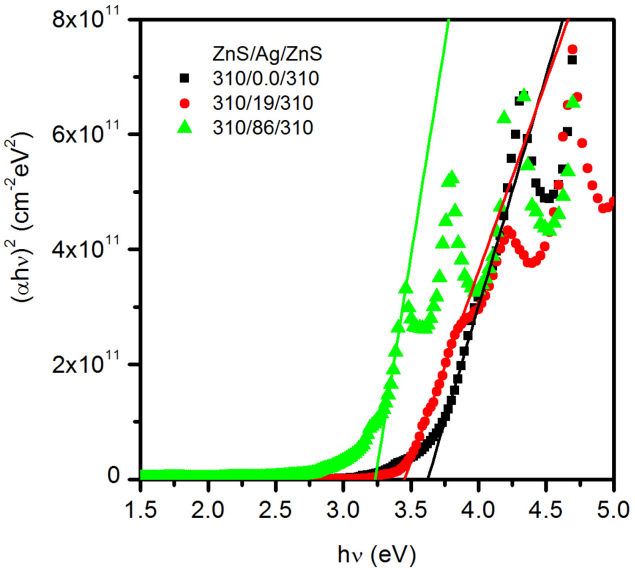

Fig. 7. $(\alpha h\nu)^2$ versus $h\nu$ plots of ZnS/Ag/ZnS multilayer films with different Ag thicknesses.

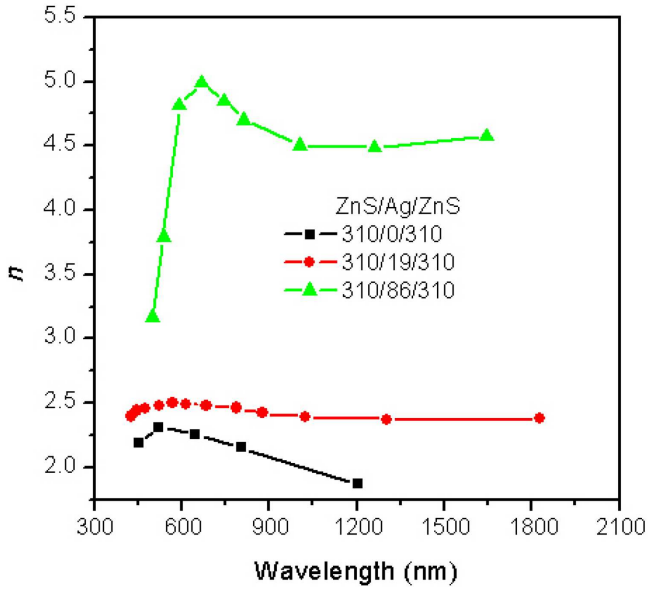

Fig. 8. Variations of the refractive index of ZnS/Ag/ZnS multilayer films with different Ag thicknesses as functions of wavelength.

effects which leads to shifting the valence band upward and shifting of the conduction band downward, and thereby resulting in band gap decreasing.

The refractive index values of ZnS/Ag/ZnS multilayer system, calculated using the Swanepoel method, are shown in Fig. 8. It is observed that the refractive index increases with increasing Ag layer thickness. Since the density of Ag is much higher than the density of ZnS, the increase in refractive index ZnS/Ag/ZnS multilayer system may be ascribed to the increase in the overall density and polarizability of ZnS/Ag/ZnS multilayer system.

4. Conclusions

ZnS thin films with different thicknesses and ZnS/Ag/ZnS multilayer films with different Ag layer thicknesses have been successfully grown on glass substrates using thermal evaporation. XRD measurements reveal that ZnS films deposited with different thicknesses have (111) preferred orientation and the intensity of the diffraction peak and the grain size increased with increasing thickness. The ZnS thickness has great influence on the optical properties. The E_g values decreased while the n values increased with increase of ZnS thickness. Also, by controlling the Ag layer thickness, the structural and optical properties of ZnS/Ag/ZnS multilayer films can be tailored. The grain size and the E_g values decreased with increasing Ag layer thickness while n values increased. By controlling the ZnS or Ag layer thicknesses. a suitable buffer layer for Cu(In,Ga)Se_2 solar cells applications can be obtained.

References

[1] R. Hernández Castillo, M. Acosta, I. Riech, G. Santana-Rodríguez, J. Mendez-Gamboa, C. Acosta, M. Zambrano, *Optik* **148**, 95 (2017).

[2] X. Yang, B. Chen, J. Chen, Y. Zhang, W. Liu, Y. Sun, *Mater. Sci. Semicond. Process.* **74**, 309 (2018).

[3] J. Cui, X. Zeng, M. Zhou, C. Hu, W. Zhang, J. Lu, *J. Lumin.* **147**, 310 (2014).

[4] X. Fang, Y. Bando, U.K. Gautam, T. Zhai, H. Zeng, X. Xu, M. Liao, D. Golberg, *Crit. Rev. Solid State Mater. Sci.* **34**, 190 (2009).

[5] J. Wu, W. Shen, H. Li, X. Liu, P. Gu, *Chin. Opt. Lett.* **8**, 32 (2010).

[6] J. Videl, O. deMelo, O. Vigil, N. Lopez, G. Contreras-Puente, O. Zelaya-Angel, *Thin Solid Films* **419**, 118 (2002).

[7] B. von Roedern, *Mater. Res. Soc. Symp. Proc.* **668**, H6.9.1 (2001).

[8] D.H. Hwang, J.H. Ahn, K.N. Hui, K.S. Hui, Y.G. Son, *Nanoscale Res. Lett.* **7**, 26 (2012).

[9] B.D. Cullity, *Elements of X-Ray Diffraction*, 2nd ed., Addison-Wesley, Reading (MA) 1979, p. 102.

[10] B.D. Cullity, S.R. Stock, *Elements of X-Ray Diffraction*, 3rd ed., Prentice-Hall, Englewood Cliffs (NJ) 2001, p. 167.

[11] M.Y. Nadeem, W. Ahmed, *Turk. J. Phys.* **24**, 651 (2000).

[12] S.H. Mohamed, M. El-Hagary, M. Emam-Ismail, *J. Phys. D Appl. Phys.* **43**, 075401 (2010).

[13] P. Prathap, N. Revathi, Y.P. Venkata Subbaiah, K.T. Ramakrishna Reddy, *J. Phys. Condens. Matter* **20**, 035205 (2008).

[14] O.K. Echendu, I.M. Dharmadasa, *J. Electron. Mater.* **43**, 791 (2014).

[15] R. Swanepoel, *J. Phys. E Sci. Instrum.* **16**, 1214 (1983).

[16] S.H. Mohamed, E.R. Shaaban, *Mater. Chem. Phys.* **121**, 249 (2010).

[17] F. Fenske, B. Selle, M. Birkholz, *Jpn. J. Appl. Phys.* **44**, L662 (2005).

[18] S.H. Mohamed, *J. Phys. Chem. Solids* **69**, 2378 (2008).

[19] H. Han, N.D. Theodore, T.L. Alford, *J. Appl. Phys.* **103**, 013708 (2008).

[20] A. Indluru, T.L. Alford, *J. Appl. Phys.* **105**, 123528 (2009).

[21] M. Raaif, S.H. Mohamed, *Appl. Phys. A* **123**, 441 (2017).

[22] M.A. Awad, M. Raaif, *J. Mater. Sci. Mater. Electron.* **29**, 2815 (2018).